American Mineralogist, Volume 89, pages 1673–1679, 2004

Crystal nucleation in hydrous rhyolite: Experimental data applied to classical theory

JULIA E. HAMMER*

Department of Geology and Geophysics, University of Hawaii, 1680 East-West Road, Honolulu, Hawaii 96822, U.S.A.

ABSTRACT

Feldspar nucleation rate data obtained by laboratory decompression of hydrous silicate melt are interpreted in view of the classical theory of nucleation (CNT) and a non-classical variation, the diffuse-interface theory (DIT). The nucleation rate data can be modeled by the CNT formalism only if the interfacial free energy (σ) is allowed to vary as a function of composition. The values thus obtained vary by a factor of four (0.024–0.100 J/m^2) and decrease systematically over a sixfold increase in dissolved H_2O content (0.8–4.8 wt%). This result is qualitatively consistent with the effects of dissolved H_2O on the liquid-vapor interfacial free energy in haplogranite magma (Mangan and Sisson 2000) and the liquid-crystal interfacial free energy in the one-component Li-disilicate system (Davis et al. 1997).

The DIT states that the interfacial region between the bulk solid and bulk melt has thermodynamic properties intermediate between these phases, and that σ is defined as the difference between the interfacial enthalpy (H_{int}) and interfacial entropy (TS_{int}). If the DIT model is correct, the nucleation rate data for feldspar may indicate that: (1) dissolved H_2O content controls the spatial distribution of enthalpy and configurational entropy around incipient crystals, and (2) the spatial gradients of these potentials diverge during devolatilization.

This study suggests that crystal nucleation studies may yield insights into the structure and thermodynamics of hydrous melts; likewise, experimental studies are important for refining a physical understanding of nucleation phenomena. Our results can be applied to quantitative numerical models of ascent-driven magma crystallization.

INTRODUCTION

Examination of natural volcanic products shows that because crystal nucleation rate determines crystal number density and ultimately crystal size distributions, it governs the texture of crystallized materials (Brandeis and Jaupart 1987; Kirkpatrick 1981; Lofgren 1980; Toramaru 2001). It is also the least understood aspect of crystallization in magmatic systems, in which melt composition and structure evolve during crystallization. Experimental studies of nucleation kinetics in silicate melts have traditionally focused on low-pressure, cooling-induced crystallization of terrestrial and lunar basalts (Baker and Grove 1985; Berkebile and Dowty 1982; Lofgren 1974, 1983), rhyolites (Fenn 1977; London 1992; Swanson 1977), and simple systems (Davis et al. 1997; Deubener 2000; James et al. 1997). Numerical treatments of thermodynamically well-characterized simple systems are starting to yield insights into the transient period before crystals are detectable (Davis and Ihinger 2002).

Effective undercooling by H_2O loss is another mechanism for crystallization in which the thermodynamic driving force is the progressive increase in the liquidus temperature accompanying devolatilization (Westrich et al. 1988). This mechanism has been studied recently in natural arc magmas, where it is recognized as an important contribution to changing melt composition and magma rheology during volcanic eruptions (Cashman and Blundy 2000; Hammer et al. 1999; Kuritani 1999; Nakada et al. 1995; Simakin et al. 2000). Thus, it is crucial to study crystallization in hydrous magmas undergoing decompression and devolatilization for application to volcanological problems. The ability to forward model crystallization rates and textures that develop during magma ascent requires an understanding of the thermodynamic driving forces as well as the kinetics of all the relevant reactions and phase transformations. We approach the challenge of uniquely interpreting volcanic processes from the textures of erupted products by collecting experimental data for natural magma compositions and critically examining classic physical models of these fundamental processes. In this paper, the results from an experimental study (Hammer and Rutherford 2002) are analyzed in the context of classical and non-classical theoretical views of crystal nucleation to investigate thermodynamic controls on feldspar nucleation in H_2O-saturated silicate melts.

METHODS

Natural dacite from the 1991 eruption of Mt. Pinatubo was selected as the starting material for an experimental study of decompression-induced crystallization because syn-eruptive crystallization due to decompression and devolatilization may have modulated this 50 h eruption sequence (Hammer et al. 1999; Polacci et al. 2001). This material is phenocryst-rich (~45 vol%) and has rhyolite matrix glass composition (78 wt% SiO_2). With respect to crystal nucleation during experimental runs, the system of interest is the hydrous interstitial melt from which feldspar grew upon devolatilization. Nucleation rate information was gathered for the most abundant nucleating phase, plagioclase feldspar (An_{40-20}) (Hammer and Rutherford 2002). In addition to nucleation of new crystals, crystallization occurred by growth of pre-existing phenocrysts. Crystal growth phenomena are beyond the scope of this paper, and are not considered further.

The experiments analyzed in this study comprise Series A runs of Hammer and Rutherford (2002); the reader is referred to that paper for a detailed description of techniques. In summary, crushed dacite pumice with sufficient distilled water

* E-mail: jhammer@hawaii.edu

added to ensure saturation at the starting pressure was brought to 780 °C and 220 MPa in cold-seal hydrothermal pressure vessels. The charges were held at these initial conditions for 24 hours, rapidly decompressed to final pressure (130, 100, 75, 50, 40, 25, 10, or 5 MPa), held for 168 hours, and then quenched.

Minerals and glasses of matrix materials were analyzed by EPMA, and quantitative textural data were obtained using digital BSE imagery and established stereological techniques (Hammer et al. 2000; Russ 1986). Feldspar nucleation rate was determined as the number of microlites per unit volume of matrix divided by the duration at low pressure. Rates obtained are thus integrated over the entire crystallization interval. They are significantly less than the initial nucleation rates following decompression as determined from shorter-duration experiments (Hammer and Rutherford 2002), because progressive crystallization in the charges reduced the effective undercooling driving solidification over time.

A primary objective of this study was to place the results of these decompression experiments into the framework of the classical theory of nucleation, which was developed using isobaric cooling experiments on molten metals (Christian 1965; Turnbull 1952). To facilitate this, the effective undercooling (ΔT_{eff}) experienced by these samples was computed as the difference between the experimental temperature (780 °C) and the feldspar liquidus temperature at the experimental pressure. In this case, the feldspar liquidus curve was obtained by assuming that it is parallel to the H_2O-saturated liquidus for the system $NaAlSi_3O_8$-H_2O (Tuttle and Bowen 1958), and passes through two points for which the liquidus temperature and pressure for the relevant melt and feldspar compositions are known: 825 °C and 100 MPa (James and Hamilton 1969), and 780 °C and 160 MPa (Hammer and Rutherford 2003).

Results

Nucleation rates obtained for each experiment and calculations of corresponding ΔT_{eff}, dissolved H_2O content, and liquid viscosity are given in Table 1. Feldspar nucleation rates vary over two orders of magnitude, ranging from 3×10^7 to 4×10^9 1/(m^3·s), with the maximum occurring at intermediate pressure corresponding to $\Delta T_{eff} \approx 165$ °C. Uncertainty in nucleation rate is ~40% relative, and is assessed as one standard deviation from the average of several processed BSE images. The high groundmass crystallinity of the charges precluded direct measurement of dissolved H_2O content, so an empirical solubility model (Moore et al. 1998) was used in combination with measured glass compositions (Hammer and Rutherford 2002) to calculate the dissolved H_2O content in melts at the experimental pressures. Dissolved H_2O content is the most important factor controlling melt viscosity; viscosity was calculated at the experimental temperature using an empirical non-Arrhenian model for rhyolite melts (Hess and Dingwell 1996).

Classical theory

The classical view of nucleation is that crystal-like clusters of atoms, possessing properties of the bulk phases, form by random fluctuations in a homogeneous one-component melt held below its liquidus temperature (Becker and Doring 1935; Volmer and Weber 1926). The excess free energy associated with maintaining the crystal/liquid interface causes clusters below a critical size to shrink and those above it to grow to macroscopic size. The steady state rate equation for the formation of critical nuclei [I(1/(m^3·s))] as a function of temperature according to the classical theory of nucleation (CNT) has the form (James 1985):

$$I = A\exp\left[\frac{-(\Delta G^* + \Delta G_D)}{k_B T}\right]; \Delta G^* = \frac{16\pi\sigma^3}{3\Delta G_V^{\,2}} S(\theta)$$
$$S(\theta) = \frac{(2+\cos\theta)(1-\cos\theta)^2}{4} \quad (1)$$

Here, the pre-exponential factor A includes the frequency of attachment attempts and the specific number density of reactant atoms in the melt ($A = k_B T n_v/h$; where k_B is the Boltzman constant, T is temperature, n_v is the volumetric concentration of reactant atoms, and h is Planck's constant), ΔG^* is the free energy required to form a spherical critical nucleus having bulk properties; σ is the free energy associated with the crystal-liquid interface, ΔG_V is the bulk free energy change per volume of the transformation, defined $\Delta G_V = \Delta G/V_M$, where V_M is the molar volume of the crystallizing phase and ΔG is the bulk free energy decrease driving solidification), ΔG_D is the activation energy required for the attachment of atoms to a cluster (a kinetic barrier), and θ is the wetting angle between the nucleus-wall and nucleus-liquid interfaces.

In the event that nucleation is homogeneous, $S(\theta) = 1$ and the thermodynamic barrier is simply a function of the volumetric free energy difference between liquid and solid (James 1985). Heterogeneous crystal nucleation is rare in metals and alloys, but common in analogous silicate systems (Greer and Kelton 1991; James 1974). There was no evidence of bubbles nor of co-precipitation of plagioclase with another mineral, and only crystals from the interior of the charges were considered in this study. However, it is possible and perhaps likely that fragments of other phases served as sites on which plagioclase nucleation occurred. [Growth on existing plagioclase fragments was observed and quantified in Hammer and Rutherford (2002).] As a result, we cannot be confident that all the groundmass plagioclase crystals formed as a result of homogeneous nucleation.

Several simplifying assumptions are needed to compare experimental data with the CNT. The first of these is that activation energy of atomic jumps across the liquid-nucleus interface is the same as that of shear relaxation of the liquid [i.e., the Stokes-Einstein approximation; Ree and Eyring (1958), Dingwell and Webb (1989)], allowing ΔG_D to be expressed in terms of viscosity (η). Following Christian (1965):

Table 1. Experimental results and calculations

Run	P_f (MPa)	H_2O (wt%)	ΔT_{eff} (°C)	I, nucleation rate [microlites 1/(m^3·s)] (1 S.D.)		η, melt viscosity (Pa·s)	σ′, interfacial free energy (J/m^{-2})
P08	5	0.8	212	3.10E+7	(9.30E+6)	1.12E+8	0.1001
P07	10	1.2	187	3.97E+9	(1.78E+9)	2.71E+7	0.0897
P02	25	2.0	140	3.81E+9	(2.03E+9)	3.91E+6	0.0751
P06	40	2.6	111	1.72E+9	(4.13E+8)	1.38E+6	0.0652
P13	50	3.0	95	6.17E+8	(2.17E+8)	8.23E+5	0.0594
P11	75	3.7	68	4.54E+8	(2.99E+8)	3.41E+5	0.0479
P04	100	4.3	46	7.70E+7	(2.82E+7)	1.81E+5	0.0375
P10	130	4.9	24	3.30E+7	(2.06E+7)	1.03E+5	0.0245

Notes: All experiments were decompressed from the same initial pressure (220 MPa) after a 24 hour equilibration period, then held at the final pressure (P_f) indicated for 168 hours. Experiments were run isothermally (780 °C).

$$\Delta G_D = -k_B T \ln\left(\frac{h}{\lambda^3 3\pi\eta}\right) \quad (2)$$

where λ is the atomic jump distance. Combined with the pre-exponential terms, the rate equation for homogenous crystal nucleation becomes:

$$I = \frac{A_c}{\eta} T \exp\left(\frac{-\Delta G^*}{k_B T}\right) A_c = \frac{n_V k_B}{3\pi\lambda^3} \quad (3)$$

Second, for a crystal-liquid system at the liquidus temperature, the thermodynamic driving force ΔG for crystallization is defined by Turnbull's approximation:

$$\Delta G = \frac{\Delta H \Delta T}{T_L} \quad (4)$$

The temperature dependence of ΔC_P for the phase change of solidification should be taken into account to accurately compute ΔG, but for small undercoolings $\Delta C_P \approx 0$ and the additional terms vanish. In the absence of the appropriate calorimetric data, we follow James (1985) and invoke Equation 4, noting that the validity of this assumption decreases as ΔT increases. Finally, an additional substitution is required to use the CNT because the present experiments are isothermal ($\Delta T = 0$). The driving force for crystallization is a change in composition (concentration of dissolved H_2O, c_{H_2O}) caused by decompression. Because the effect of devolatilization on the liquidus temperature is embedded in the above definition of effective undercooling, ΔT_{eff}, this derived parameter is inserted into Equation 4 in place of ΔT to estimate the magnitude of ΔG imposed by decompression and devolatilization.

The crystal-liquid interfacial free energy (σ), with units of energy per unit area, is distinct from the one-dimensional (energy per unit length) surface tension used in the description of bubble nucleation (also commonly denoted as "σ"). It is a key parameter in the CNT that is exceedingly difficult to obtain independently from nucleation data. The few such values in existence were derived from measurements of crystal-melt dihedral angles (Cooper and Kohlstedt 1982; Ikeda et al. 2002; Rose and Brenan 2001) and numerical studies of hard-sphere molecular interaction potentials (Battezzati 2001; Davidchack and Laird 2003; Granasy et al. 2002); there are no crystal-melt σ data for natural, hydrous silicate melts with coexisting feldspar. One method of obtaining σ for the case of homogeneous nucleation is to assume the CNT is valid and determine its value from the slope of a plot of $[1/(T\Delta G_V^2)]$ vs. ln $(I\,\eta/T)$ (Gonzalez-Oliver and James 1980). However, for the data analyzed here, the terms are not well described by a linear correlation ($r^2 = 0.59$), and thus the CNT in its original form does not adequately describe these data.

Another common approach is to consider the possibility that the form of the CNT is correct but that the interfacial energy is not single-valued (Greer and Kelton 1991; James 1974). Rearranging Equation 3 to solve for σ using nucleation rate data, a separate value for each experiment may be calculated. In the event of heterogeneous nucleation, it is impossible to solve for σ in this way without knowledge of θ. For the present purposes, in which both σ and θ are completely unconstrained, we provisionally take $S(\theta) = 1$ (Eq. 1), and find a value of σ corresponding to each of the nucleation rate measurements (Table 1). The result is expressed as σ' to acknowledge that the free energy thus obtained incorporates any reduction in the barrier to nucleation due to the presence of additional phases and submicroscopic crystalline substrates.

The computed interfacial free energies are not constant, but vary by a factor of four and decrease systematically with increasing H_2O content over the range ~1–5 wt% (Fig. 1c). A factor of 2.5 increase in dissolved H_2O content appears to have caused σ to decrease by a factor of five and nucleation rate to increase by about two orders of magnitude. A qualitatively similar result

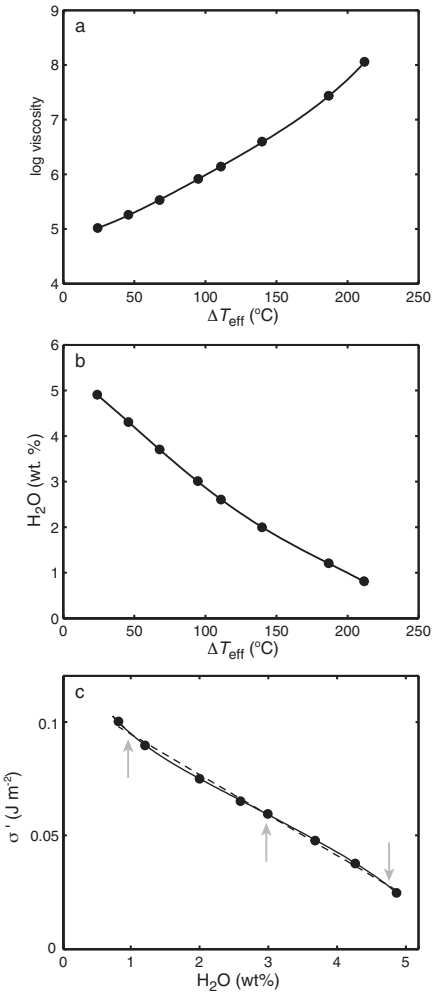

FIGURE 1. Parameters calculated for each experiment (filled circles, values in Table 1) and corresponding polynomial fits (solid curves) used in the calculation of nucleation rate according to classical theory (Eq. 3). Viscosity **(a)** and dissolved H_2O content **(b)** calculated using the empirical models of Hess and Dingwell (1996) and Moore (1998), respectively. Estimated uncertainty in ΔT_{eff} is ±10 °C. Interfacial free energy, σ in **(c)** solved by rearranging Equation 3; other parameter values used in calculation are: V_M, = 1.003×10^{-4} m^3/mol (calculated for An_{30} as a linear combination of albite and anorthite values (Klein 1994)), $\lambda = 3 \times 10^{-10}$ m, ΔH_f for An_{30} plagioclase at 200 MPa P_{H_2O} = 74 300 J/mol (Burnham and Nekvasil 1986; Muncill and Lasaga 1988), $n_V = N_A/V_M$ (N_A = Avogadro constant). Fit equations shown are: $\sigma = -0.0176 \cdot (H_2O) + 0.1121$ (solid curve), and $\sigma = -0.0001 \cdot (H_2O)^5 + 0.0016 \cdot H_2O)^4 - 0.0100 \cdot (H_2O)^3 + 0.0308 \cdot (H_2O)^2 - 0.0633 \cdot (H_2O) + 0.1354$ (dashed line).

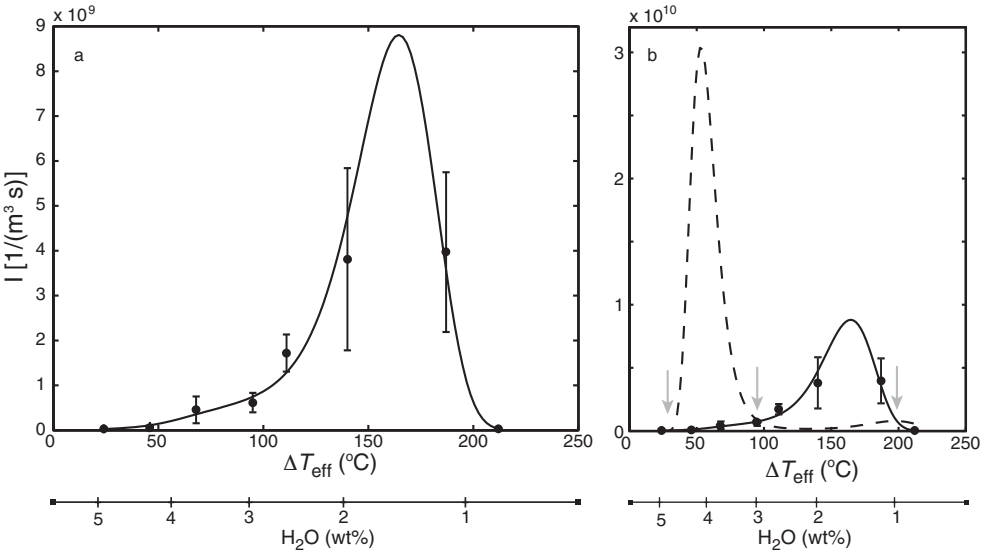

FIGURE 2. Experimental nucleation rate data (symbols) and model rates (curves) found using Equation 3. **(a)** CNT curve calculated using parameter values shown in Figure 1 with 5th order polynomial σ-H_2O expression. **(b)** CNT curve calculated using linear σ-H_2O expression shown for comparison (dashed curve). Note shifts in magnitude and location of the nucleation rate maximum.

was obtained for the behavior of σ with dissolved H_2O in the H_2O-$Li_2Si_2O_5$ system (Davis et al. 1997), although the concentrations of H_2O examined were much smaller. In that study, an order- of- magnitude increase in H_2O content (from 130 to 975 ppm) is correlated with an increase in the crystal nucleation rate of two orders of magnitude.

What might cause this compositional dependence of nucleation rate on nucleation kinetics? Heslin and Shelby (1993) suggested that the influence of H_2O on nucleation in Li- disilicate is strictly a result of the viscosity dependence on H_2O content, and is thus a factor influencing the kinetic barrier to atomic attachment. A viscosity effect is not solely responsible for the apparent σ-H_2O relationship in this case, since melt viscosity consistently decreases with increasing H_2O content whereas the observed nucleation rates do not (Table 1). Here, H_2O loss provides a chemical driving force for crystallization, and we surmise therefore that devolatilization affects the free energy term in the nucleation rate equation.

Given adequate expressions for the co-variation of viscosity, H_2O content, σ, and ΔT_{eff} (Fig. 1), the full nucleation rate curve can be calculated for this system according to a modified (i.e., σ-varying) CNT expression (Fig. 2a). The calculated curve is bell-shaped, as expected, with the location of maximum nucleation rate at 165 °C effective undercooling. At all values of ΔT_{eff}, the calculated nucleation rate is within the error estimates for the data, and the curve fits the data well ($r^2 = 0.924$). Notably, the maximum nucleation rate for this system as indicated by the CNT, 8.8×10^9 1/(m^3·s), is about twice the maximum observed rate, 3.8×10^9 1/(m^3·s).

Of course, a good fit to the nucleation data by the rate equation (Eq. 3) is a foregone conclusion because σ' was treated as an adjustable parameter in formulating the rate equation. One possibility is that σ', as calculated, has no physical meaning and simply accumulates errors associated with the model assumptions. Although this possibility cannot be eliminated, a compositional control on nucleation kinetics is suggested by the systematic σ'-H_2O trend shown in Figure 1c. It is worth noting that the approximately linear σ'-H_2O relationship is not the result of circularity. The rate data (used to determine σ') do not vary linearly with melt viscosity, ΔT_{eff}, or c_{H_2O} (Table 1). The objective of interpreting these data further is that theory provides a basis for investigating the underlying physical chemistry of solidification.

Forward calculation of nucleation rate values using the CNT is extremely sensitive to the expression for σ'. If a linear (rather than 5th-order polynomial) σ'-H_2O relationship is used in computing the nucleation rate curve, the maximum rate obtained increases by a factor of 3.4 (dashed curve Fig. 2b). Even more importantly, the position of the maximum is displaced to lower effective undercooling (ΔT_{eff} ~100 degrees below observation), and the correlation between the nucleation curve and data becomes statistically insignificant ($r^2 = 0.161$). These discrepancies may seem intuitively disproportionate. It may be helpful to compare the crossover points in the two nucleation rate predictions (marked with arrows in Fig. 2b) with the crossover points in σ' shown in Figure 1c (but note difference in x-axis directions). For H_2O concentrations where the linear fit produces greater σ' values, the corresponding nucleation rate is lower than observed, and vice versa. The differences arise from the extreme sensitivity of nucleation rate on σ' that is inherent to the CNT. In combination with theory, nucleation rate experiments provide a means of computing σ' (James 1974; Zanotto and James 1985). The converse is not true; σ' data must be fantastically precise to predict nucleation behavior.

NON-CLASSICAL THEORY

Key assumptions at the heart of the CNT are (1) a critical nucleus has the thermodynamic properties of the bulk solid; (2) the interface between nucleus and melt is a sharp boundary; and (3) regardless of critical cluster size, the nucleus-liquid interfacial free energy can be treated as a macroscopic property equal to the value for a planar interface. These assumptions have been implicated in the failure of the CNT to describe nucleation kinetics for a variety of systems (Greer and Kelton 1991; James 1985). One alternative

has been to incorporate variation in σ as a function of temperature (Zanotto and James 1985), roughness (Sen and Mukerji 1999), or interface curvature and thus particle size (Weinberg et al. 1992). The approach taken here is to consider a non-classical theory that posits a spatial distribution of thermodynamic properties in the vicinity of clusters (Turnbull 1964). In essence, this model takes into account gradations between bulk-solid and bulk-liquid values of enthalpy and entropy within an interface region. This region is not a separate phase, but rather a transitional interval that exists solely because solid and liquid surround it.

This diffuse interface theory (DIT) works well in explaining the temperature dependence of σ in various systems (e.g., $Li_2O{\cdot}2SiO_2$, $BaO{\cdot}\ 2SiO_2$, Hg, etc.; Granasy 1993; Spaepen 1994). The model states that relative to the bulk melt and cluster center (which possesses properties of a bulk solid), the crystal-melt interfaces are regions in which excess free energy (σ) increases to a maximum at some radial distance from the center of a subcritical cluster. In contrast to crystal-crystal boundaries, which are sharply defined regions of large enthalpy due to a high density of broken bonds, cluster-liquid interfacial regions contain a lower density of broken bonds. Bonding arrangements in this region are somewhat similar to those in the neighboring solid (Spaepen 1994). Because undercooling a melt to produce glass is impossible without positive interfacial free energy [otherwise there would be no thermodynamic barrier to crystallization (Turnbull 1952)], the interfacial free energy, defined as H_{int}–TS_{int} must be greater than zero. Thus, the energetic contribution of enthalpy (H_{int}) must increase more steeply than entropy (TS_{int}) with radial distance from the nucleus (Fig. 3).

In essence, this thermodynamic description implies that at a given radial distance from the core of an atomic cluster, the solid exerts a structural (enthalpic) influence into the melt, yet the atomic configuration (entropy) within the region more closely resembles a liquid than a solid. According to this model, σ' varies spatially within the diffuse interfacial region (Fig. 3a). In practice, only one value of σ' is obtained by solving Equation 3 for a given experiment. For simplicity, the calculated value of σ' is taken as proportional to the area under the σ'-distance curve predicted by the DIT (Fig. 3b), and conversely, the curves separate as H2O is exsolved.

The existing formulations of the DIT treat the changes in σ due to temperature variation only. However, compositional factors could profoundly influence the H_{int} and TS_{int} gradients, simply because the chemical makeup of the melt and solid control the bonding and configuration of the interface. The negative correlation between calculated σ' and H_2O (Fig. 1c) is the most striking result of the present analysis; the following discussion introduces a possible explanation for this relationship.

FELDSPAR-MELT INTERFACIAL FREE ENERGY

One interpretation holds that the magnitude of the crystal-liquid interfacial free energy is proportional to the compositional dis-similarity of the phases (Toshiya et al. 1991). In the present case, melt with little dissolved H_2O is structurally and compositionally more similar to plagioclase than is H_2O-rich melt. Thus the observed negative correlation of σ' with H_2O content (Fig. 2c) is inconsistent with this idea. Instead, the observed relationship implies that the magnitude of the difference between H_{int} and TS_{int}

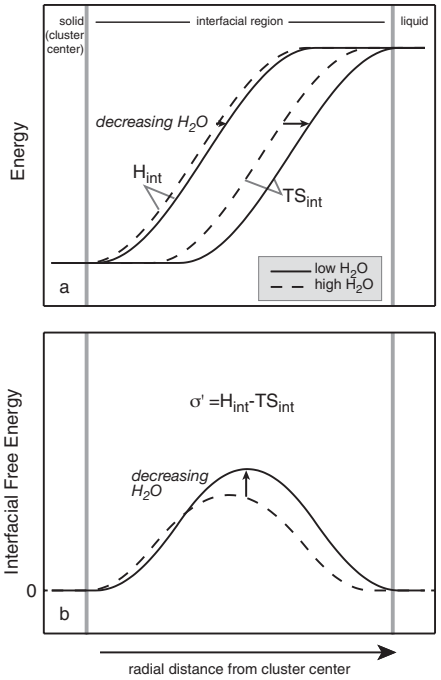

FIGURE 3. Schematic cross section of the interfacial region between a subcritical cluster and the surrounding melt showing thermodynamic properties of a diffuse interface (modified from Spaepen 1994). **(a)** Gradients in enthalpy (H_{int}) and entropy (TS_{int}) with radial distance from a subcritical cluster for H_2O-rich (dashed line) and H_2O-poor (unbroken line) melts. Materials in "solid" and "liquid" regions possess thermodynamic properties of bulk (i.e., macroscopic) phases. Area enclosed by curves in **(a)** is proportional to the interfacial excess free energy, σ, shown separately in **(b)**. The inverse σ-H_2O trend (Fig. 1c) suggests that the H_{int} and TS_{int} gradients in H_2O-rich melts are positioned closer to the "solid" than in H_2O-poor melt, and that the curves diverge during decompression and H_2O-loss. The result is an increase in the magnitude of σ with decompression; the direction and magnitude of the horizontal shift in the σ peak is arbitrary in this schematic representation.

decreases with the addition of H_2O to the system (Fig. 3b) and, conversely, the curves separate as #20 is exsolved. Separation of the curves due to H_2O loss may be the result of (1) fixed H_{int} gradient position with a shift in TS_{int} toward the cluster center; (2) fixed TS_{int} gradient with a melt-ward shift in the H_{int} curve; (3) shifts in both TS_{int} and H_{int} in opposite senses toward an intermediate point; or (4) differential shifts of both gradients in the same direction (either toward or away from the cluster center), such that the quantity (H_{int}-TS_{int}) remains positive and progressively decreases.

From solubility measurements and in situ spectroscopic observations of hydrous melts and glasses, H_2O is known to initially dissolve in silicate melt by a dissociation reaction in which tetrahedally coordinated bridging O atoms are converted to non-bridging O atoms, and local charge balance is accommodated by protons or monovalent cations (Burnham 1975). Above ~1 wt% total H_2O, molecular H_2O becomes significant (McMillan 1994; Silver and Stolper 1989), although in situ studies indicate that OH- incorporation continues to be important up to 22 wt% total H_2O (Nowak and Behrens 2001; Sowerby and

Keppler 1999). The homogenous equilibrium among dissolved molecular H_2O, O in the melt, and dissolved OH- groups may be written as an oxygen reaction:

$$\underset{\text{(free)}}{O^0} + \underset{\text{(bridging)}}{O^{2-}} = \underset{\text{(non-bridging)}}{2O^-} \quad (5)$$

As a result of dissolution as both OH- groups and molecular H_2O, the distribution of O atoms among free, bridging, and non-bridging sites is shifted toward greater non-bridging site occupancy. Increased occupancy in diverse site types could increase entropy if the dominant contribution is a configurational term sensitive to the number of equivalent microstates of the solution. This phenomenon affects the melt everywhere, not just within the interface region. For the site occupancies of O atoms to have an effect on crystal nucleation, the configurational entropy increase must be localized around incipient crystals. The local entropy around crystals could increase if slightly higher concentrations of H_2O develop in a boundary layer surrounding subcritical clusters because it is a rejected component during crystallization of anhydrous phases (Kirkpatrick 1981). Increased configurational entropy around clusters, particularly in H_2O-rich melts, would be consistent with a shift of the TS_{int} gradient toward the cluster at high H_2O contents. Melt enthalpy is also related to the oxygen reaction (Hess 1995). Thus, the H_{int} gradient may also shift toward the crystal because the structural influence of the solid into the interfacial region decreases proportionally with increasing H_2O.

If the DIT model describes the thermodynamics of the interfacial region in hydrous silicate melt, and increased H_2O content causes a shift in both the configurational energy gradient (TS_{int}) and the enthalpic energy gradient (H_{int}) toward the incipient crystal, then the observed σ-H_2O relationship may be achieved by process 4, described above. A thermodynamic feature inherent to the DIT is that H_{int} begins to increase closer to the cluster center than TS_{int} (Fig. 3a); otherwise, σ is negatively valued. The experimental data taken in the context of the DIT further indicate that with the addition of H_2O, the TS_{int} curve must shift more than the H_{int} curve to produce the observed inverse σ'-H_2O relationship (Fig. 3b). Conversely, during decompression and H_2O loss from hydrous melt, σ' progressively increases because the gradient in TS_{int} retreats from the cluster more swiftly than H_{int}.

Further tests of the DIT as a model for nucleation in hydrous silicate melt are needed. In addition to gathering additional experimental data (e.g., more values of ΔT_{eff}), including measurements of nucleation induction times, tests include finding independent evidence that the magnitude of enthalpy change with varying dissolved H_2O content is less than that of entropy. An examination of entropic and enthalpic effects of H_2O dissolution would link melt structure at a molecular scale with macroscopic thermodynamic properties and support or refute the diffuse interface model for incipient plagioclase crystals forming in hydrous silicate melts.

A second avenue of testing is to determine crystal-melt surface energies as a function of dissolved H_2O content using a method independent from nucleation kinetics experiments. Such determinations would address the validity of applying classical nucleation theory, essentially a rate equation constructed on a thermodynamic energy balance, to natural multicomponent silicate melts undergoing decompression. Correspondence of surface free energy values recently obtained for hydrous silicate melt and coexisting vapor using different experimental techniques are encouraging in this regard. Bagdassarov et al. (2000) determined values of the vapor-liquid surface free energy in hydrated haplogranite liquid by a sessile drop technique that are identical within error to values obtained by back-solving the CNT equation with bubble nucleation experimental rate data (Mangan and Sisson 2000). Another interesting and potentially relevant result of the high-pressure sessile drop experiments is a clear negative linear correlation of $\sigma_{vapor\text{-}liquid}$ and c_{H_2O}, wherein σ decreases by a factor of ~4.5 as c_{H_2O} increases from 0.2 to 10.5 wt%. Close agreement of surface energy values obtained by the nucleation rate and sessile drop techniques is one indication that the CNT formalism describes feldspar nucleation driven by H_2O loss from silicate melt. The similar negative dependence of $\sigma_{vapor\text{-}liquid}$ and $\sigma_{crystal\text{-}liquid}$ on dissolved H_2O in melt is additional support for the utility of nucleation experiments in continued examination of liquid-crystal surface free energy phenomena.

ACKNOWLEDGMENTS

I thank Malcolm J Rutherford for gracious collaboration in the laboratory. Discussions with Paul Hess, Yan Liang, and Margaret Mangan were inspiring and helpful. Rebecca Lange and Phil Ihinger provided illuminating and constructive reviews that improved the manuscript significantly. This study was supported by National Science Foundation award EAR-0234071. This is SOEST publication no. 6390.

REFERENCES CITED

Bagdassarov, N., Dorfman, A., and Dingwell, D.B. (2000) Effect of alkalis, phosphorus, and water on the surface tension of haplogranite melt. American Mineralogist, 85, 33–40.

Baker, M.B. and Grove, T.L. (1985) Kinetic controls on pyroxene nucleation and metastable liquid lines of descent in a basaltic andesite. American Mineralogist, 70, 279–287.

Battezzati, L. (2001) Thermodynamic quantities in nucleation. Materials Science and Engineering a—Structural Materials Properties Microstructure and Processing, 304, 103–107.

Becker, R. and Doring, W. (1935) Kinetische behandlung der keim buildung in ubersattingten dampfen. Annalen der Physik, 5, 719–752.

Berkebile, C.A. and Dowty, E. (1982) Nucleation in laboratory charges of basaltic composition. American Mineralogist, 67, 886–899.

Brandeis, G. and Jaupart, C. (1987) The kinetics of nucleation and crystal growth and scaling laws for magmatic crystallization. Contributions to Mineralogy and Petrology, 96, 24–34.

Burnham, C.W. (1975) Water and magmas: a mixing model. Geochimica et Cosmochimica Acta, 39, 1077–1084.

Burnham, C.W. and Nekvasil, H. (1986) Equilibrium properties of granite pegmatite magmas. American Mineralogist, 71, 239–263.

Cashman, K. and Blundy, J. (2000) Degassing and crystallization of ascending andesite and dacite. Philosophical Transactions of the Royal Society of London Series A, 358(1770), 1487–1513.

Christian, J.W. (1965) The Theory of Transformations in Metals and Alloys, 973 p. Pergamon Press, New York.

Cooper, R.F. and Kohlstedt, D.L. (1982) Interfacial energies in the olivine-basalt system. In S. Akimoto, and M.H. Manghnani, Eds., High-Pressure Research in Geophysics, 12, p. 217–228. D. Reidel Publishing Co., Tokyo.

Davidchack, R.L. and Laird, B.B. (2003) Direct calculation of the crystal-melt interfacial free energies for continuous potentials: Application to the Lennard-Jones system. Journal of Chemical Physics, 118, 7651–7657.

Davis, M.J. and Ihinger, P.D. (2002) Effects of thermal history on crystal nucleation in silicate melt: Numerical simulations. Journal of Geophysical Research-Solid Earth, 107(B11), art. no.-2284.

Davis, M.J., Ihinger, P.D., and Lasaga, A.C. (1997) Influence of water on nucleation kinetics in silicate melt. Journal of Non-Crystalline Solids, 219, 62–69.

Deubener, J. (2000) Compositional onset of homogeneous nucleation in (Li, Na) disilicate glasses. Journal of Non-Crystalline Solids, 274, 195–201.

Dingwell, D.B. and Webb, S.L. (1989) Structural relaxation in silicate melts and non-Newtonian melt rheology in geologic processes. Physics and Chemistry of Minerals, 16, 508–516.

Fenn, P.M. (1977) The nucleation and growth of alkali feldspar from hydrous melts.

The Canadian Mineralogist, 15, 135–161.
Gonzalez-Oliver, C.J.R. and James, P.F. (1980) Crystal nucleation and growth in a Na_2O-2CaO-3SiO_2 glass. Journal of Non-Crystalline Solids, 38/39, 699–704.
Granasy, L. (1993) Diffuse Interface Theory of Nucleation. Journal of Non-Crystalline Solids, 162, 301–303.
Granasy, L., Pusztai, T., and James, P.F. (2002) Interfacial properties deduced from nucleation experiments: A Cahn-Hilliard analysis. Journal of Chemical Physics, 117, 6157–6168.
Greer, A.L. and Kelton, K.F. (1991) Nucleation in Lithium Disilicate Glass—a Test of Classical- Theory By Quantitative Modeling. Journal of the American Ceramic Society, 74, 1015–1022.
Hammer, J.E. and Rutherford, M.J. (2002) An experimental study of the kinetics of decompression-induced crystallization in silicic melt. Journal of Geophysical Research, 107(B1), 10.1029/2001JB00281.
——— (2003) Petrologic indicators of preeruption magma dynamics. Geology, 31, 79–82.
Hammer, J.E., Cashman, K.V., Hoblitt, R.P., and Newman, S. (1999) Degassing and microlite crystallization during pre-climactic events of the 1991 eruption of Mt. Pinatubo, Philippines. Bulletin of Volcanology, 60, 355–380.
Hammer, J.E., Cashman, K.V., and Voight, B. (2000) Magmatic processes revealed by textural and compositional trends in Merapi dome lavas. Journal of Volcanology and Geothermal Research, 100, 165–192.
Heslin, M.R. and Shelby, J.E. (1993). In C. Weinberg, Ed., Ceramic Transactions, 30. American Ceramic Society, Westerville.
Hess, K.U. and Dingwell, D.B. (1996) Viscosities of hydrous leucogranitic melts: A non-Arrhenian model. American Mineralogist, 81, 1297–1300.
Hess, P.C. (1995) Thermodynamic mixing properties and the structure of silicate melts. Structure, Dynamics and Properties of Silicate Melts, 32, p. 145–189.
Ikeda, S., Toriumi, M., Yoshida, H., and Shimizu, I. (2002) Experimental study of the textural development of igneous rocks in the late stage of crystallization: the importance of interfacial energies under non-equilibrium conditions. Contributions to Mineralogy and Petrology, 142, 397–415.
James, P.F. (1974) Kinetics of crystal nucleation in lithium silicate glasses. Physics and Chemistry of Glasses, 15, 95–105.
——— (1985) Kinetics of crystal nucleation in silicate glasses. Journal of Non-Crystalline Solids, 73, 517–540.
James, P.F., Iqbal, Y., Jais, U.S., Jordery, S., and Lee, W.E. (1997) Crystallisation of silicate and phosphate glasses. Journal of Non-Crystalline Solids, 219, 17–29.
James, R. and Hamilton, D. (1969) Phase relations in the system $NaAlSi_3O_8$-$KAlSi_3O_8$-$CaAl_2Si_2O_8$-SiO_2-H_2O at 1 kb water vapor pressure. Contributions to Mineralogy and Petrology, 21, 111–141.
Kirkpatrick, R.J. (1981) Kinetics of Crystallization of Igneous Rocks. In A. Lasaga, and R. Kirkpatrick, Eds., Kinetics of Geochemical Processes, 8, p. 321–397. Mineralogical Society of America, Washington, D.C.
Klein, C. (1994) Mineral Science, 641 p. Wiley, New York.
Kuritani, T. (1999) Phenocryst crystallization during ascent of alkali basalt magma at Rishiri Volcano, northern Japan. Journal of Volcanology and Geothermal Research, 88, 77–97.
Lofgren, G. (1974) An experimental study of plagioclase crystal morphology: isothermal crystallization. American Journal of Science, 274, 243–273.
——— (1983) Effect of heterogeneous nucleation on basaltic textures; a dynamic crystallization study. Journal of Petrology, 24, 229–255.
Lofgren, G.E. (1980) Experimental studies on the dynamic crystallization of silicate melts. In R. Hargraves, Ed., Physics of Magmatic Processes, p. 487–551. Princeton University Press, New Jersey.
London, D. (1992) The application of experimental petrology to the genesis and crystallization of granitic pegmatites. Canadian Mineralogist, 30, 499–540.
Mangan, M. and Sisson, T. (2000) Delayed, disequilibrium degassing in rhyolite magma: decompression experiments and implications for explosive volcanism. Earth and Planetary Science Letters, 183, 441–455.
McMillan, P.F. (1994) Water Solubility and Speciation Models. Volatiles in Magmas, 30, p. 131–156.
Moore, G., Vennemann, T., and Carmichael, I.S.E. (1998) An empirical model for the solubility of H_2O in magmas to 3 kilobars. American Mineralogist, 83, 36–42.
Muncill, G.E. and Lasaga, A.C. (1988) Crystal-growth kinetics of plagioclase in igneous systems: Isothermal H_2O-saturated experiments and extension of a growth model to complex silicate melts. American Mineralogist, 73, 982–992.
Nakada, S., Motomura, Y., and Shimizu, H. (1995) Manner of magma ascent at Unzen Volcano (Japan). Geophysical Research Letters, 22, 567–570.
Nowak, M. and Behrens, H. (2001) Water in rhyolitic magmas: getting a grip on a slippery problem. Earth and Planetary Science Letters, 184, 515–522.
Polacci, M., Papale, P., and Rosi, M. (2001) Textural heterogeneities in pumices from the climactic eruption of Mount Pinatubo, 15 June 1991, and implications for magma ascent dynamics. Bulletin of Volcanology, 63, 83–97.
Ree, T. and Eyring, H. (1958) The relaxation theory of transport phenomena. In F.R. Eirich, Ed. Rheology: theory and applications, 2. Academic Press, New York.
Rose, L.A. and Brenan, J.M. (2001) Wetting properties of Fe-Ni-Co-Cu-O-S melts against olivine: Implications for sulfide melt mobility. Economic Geology and the Bulletin of the Society of Economic Geologists, 96, 145–157.
Russ, J.C. (1986) Practical Stereology, 194 p. Plenum Publishing Corp., New York.
Sen, S. and Mukerji, T. (1999) A generalized classical nucleation theory for rough interfaces: application in the analysis of homogeneous nucleation in silicate liquids. Journal of Non-Crystalline Solids, 246, 229–239.
Silver, L. and Stolper, E. (1989) Water in Albitic Glasses. Journal of Petrology, 30, 667–709.
Simakin, A.G., Armienti, P., and Salova, T.P. (2000) Joint degassing and crystallization: Experimental study with a gradual pressure release. Geochemistry International, 38, 523–534.
Sowerby, J.R. and Keppler, H. (1999) Water speciation in rhyolitic melt determined by in-situ infrared spectroscopy. American Mineralogist, 84, 1843–1849.
Spaepen, F. (1994) Homogeneous nucleation and the temperature dependence of the crystal-melt interfacial tension. Solid State Physics—Advances in Research and Applications, vol. 47, 47, p. 1–32.
Swanson, S.E. (1977) Relation of nucleation and crystal-growth rate to the development of granitic textures. American Mineralogist, 62, 966–978.
Toramaru, A. (2001) A numerical experiment of crystallization for a binary eutectic system with application to igneous textures. Journal of Geophysical Research-Solid Earth, 106, 4037–4060.
Toshiya, A., Katsuo, T., and Ichiro, S. (1991) Nucleation, growth and stability of Ca $Al_2Si_2O_8$ polymorphs. Physics and Chemistry of Minerals, 17, 473–484.
Turnbull, D. (1952) Kinetics of solidification of supercooled liquid mercury droplets. Journal of Chemical Physics, 20, 411.
——— (1964). Thermodynamics and kinetics of formation of the glass state and initial devitrification. In J.A. Prins, Ed., Physics of non-crystalline solids, p. 667. North-Holland, Amsterdam.
Tuttle, O. and Bowen, N. (1958) Origin of Granite in Light of Experimental Studies, 153 p. Geological Society of America, Boulder, Colorado.
Volmer, M. and Weber, A. (1926) Kimbildung in ubersattingten gebilden. Zeitschrift für Physikalische Chemie, 119, 277–301.
Weinberg, M.C., Zanotto, E.D., and Manrich, S. (1992) Classical nucleation theory with a size dependent interfacial-tension-Li_2O·2SiO_2 Crystal nucleation. Physics and Chemistry of Glasses, 33, 99–102.
Westrich, H.R., Stockman, H.W., and Eichelberger, J.C. (1988) Degassing of rhyolitic magma during ascent and emplacement. Journal of Geophysical Research, 93, 6503–6511.
Zanotto, E.D. and James, P.F. (1985) Experimental tests of the Classical Nucleation Theory for glasses. Journal of Non-Crystalline Solids, 74, 373.

MANUSCRIPT RECEIVED SEPTEMBER 28, 2003
MANUSCRIPT ACCEPTED AUGUST 1, 2004
MANUSCRIPT HANDLED BY WENDY BOHRSON